Title

Axial and Radial Thermal Responses of a Field-Scale Energy Pile under Monotonic and Cyclic Temperature Changes

Journal

Journal of Geotechnical and Geoenvironmental Engineering, 144(10)

ISSN

1090-0241

Authors

Faizal, Mohammed
Bouazza, Abdelmalek
Haberfield, Chris
et al.

Publication Date

2018-10-01

DOI

10.1061/(asce)gt.1943-5606.0001952

Peer reviewed

Axial and radial thermal responses of a field scale energy pile under monotonic and cyclic temperature changes

by

Mohammed Faizal

PhD Student, Monash University, Department of Civil Engineering, 23 College Walk, Clayton, Vic. 3800, Australia. Telephone: +61 3 9905 8901; Email: mohammed.faizal@monash.edu

*** Abdelmalek Bouazza (Corresponding Author)**

Professor, Monash University, Department of Civil Engineering, 23 College Walk, Clayton, Vic. 3800, Australia. Telephone: +61 3-9905 4956, Email: malek.bouazza@monash.edu

Chris Haberfield

Principal, Golder Associates Pty. Ltd., Building 7, Botanicca Corporate Park, 570–588 Swan St., Richmond, Vic. 3121, Australia. Telephone: +61 3 8862 3586; Email: chaberfield@golder.com.au

John S. McCartney

Associate Professor, University of California San Diego, Department of Structural Engineering, 9500 Gilman Drive, SME 442J, La Jolla, CA 92093-0085, USA, Telephone: +1 858 534-9630; Email: mccartney@ucsd.edu

Abstract

The axial and radial thermal responses of a field-scale energy pile installed in dense sand and subjected to monotonic and cyclic temperatures are examined. It is found that the axial thermal strains in the pile are more restricted to thermal expansion/contraction compared to radial thermal strains. The radial thermal strains are close to that of a pile expanding/contracting freely, indicating minimal resistance from the surrounding soil in the radial direction. As a result, very low magnitudes of radial thermal stresses developed in the pile compared to axial thermal stresses. The pile-soil radial contact stresses estimated from cavity expansion analysis are up to 12 kPa for a pile temperature change of 22.5^{o}C and are likely negligible for the range of commonly-encountered operating temperatures of energy piles installed in dense sand. During cyclic heating and cooling, unstable changes in axial and radial thermal strains were observed initially during initial cycles indicating a ratcheting response. The changes in strains became more stable over further cycles, without significant changes in side friction, pile-soil contact stresses, or strength of the dense sand.

Keywords*: Energy piles; field tests; axial thermal response; radial thermal response; monotonic temperatures; cyclic temperatures.*

Introduction

Energy piles support buildings while acting as underground heat exchangers coupled with ground source heat pumps to assist in maintaining thermal comfort in built structures (Brandl, 2006; DeMoel et al., 2010; Bouazza et al., 2011). Depending on usage requirements, energy piles typically experience temperatures ranging from 10 to 35°C related to monotonic heating and cooling (Brandl, 2006; Murphy and McCartney, 2012, 2015; McCartney and Murphy 2017), including daily fluctuations in temperature resulting from intermittent operations associated with natural and forced ground thermal recharging. Ground thermal recharging involves injecting additional heat into the system while operating a heat pump to meet the cyclic heating and cooling demands of the building, and is beneficial in improving geothermal energy utilization and helps in maintaining a balance of ground temperatures (Yi et al., 2008; Wood et al., 2010; Jalaluddin and Miyara, 2012).

Temperature changes can induce volumetric changes of an energy pile and can potentially affect the interaction between the energy pile and the soil. Recent studies on field scale energy piles have assessed their thermal response mostly when they are subjected to monotonic heating (Laloui et al., 2006; Bourne-Webb et al., 2009; Akrouch et al., 2014; Mimouni, 2014; Mimouni and Laloui, 2015; Wang et al., 2015; Murphy et al., 2015; Sutman et al., 2015) or under normal seasonal heat pump operation (Brandl 2006; Murphy and McCartney 2012, 2015; McCartney and Murphy 2017). The thermal response of field scale energy piles subjected to daily cyclic temperatures under intermittent operations of a heat pump with natural ground thermal recovery has only recently started to receive interest (Faizal et al., 2016), and practically no assessments have been reported in the literature for daily cyclic temperatures resulting from forced ground thermal recharging. Frequent temperature reversals may induce different magnitudes of thermal loads in the pile and at the pile-soil interface compared to monotonic

temperature changes. Depending on the soil surrounding the energy pile, thermal cycles could cause fatigue-like processes which could intensify deformations of the pile and the surrounding soil (Suryatriyastuti et al. 2013; Olgun et al., 2014; Pasten and Santamarina 2014). Although investigated using numerical simulations for energy piles in idealized soil layers, this cyclic thermal mechanism is not well understood at a field scale.

A number of small-scale physical model studies have characterized the axial thermal response of energy piles for monotonic heating (McCartney and Rosenberg, 2011; Ng et al., 2014b; Goode and McCartney, 2015) and cyclic temperatures (Kalantidou et al., 2012; Ng et al., 2014a; Stewart and McCartney, 2014; Yavari et al., 2014, 2016a; Ng et al., 2016; Wang et al., 2016). These small-scale model studies, however, are still representative of idealized soil layers that do not represent field conditions or installation effects, and do not have sufficient space to include instrumentation to evaluate the thermal strains in the axial and radial directions. Such information requires confirmation from instrumented energy pilesi n the field.

Moreover, most previous studies on field scale energy piles have assessed their axial thermal responses under monotonic increases or decreases in temperature (Bourne-Webb et al., 2009; Akrouch et al., 2015; Murphy et al., 2015) or under actual heat pump operation (Murphy and McCartney, 2015; McCartney and Murphy, 2017), both of which do not permit a simple evaluation of the long-term effects of cyclic heating and cooling. Further, consideration of radial strains in energy piles are limited to a few studies (Laloui et al., 2006; Mimouni, 2014; Mimouni and Laloui, 2015; Wang et al., 2015, Wang, 2017). An assessment of the radial thermal response of field-scale energy piles will clarify if lateral expansion/contraction of the pile could cause pile and soil deformations under monotonic and cyclic temperatures. Evaluation of the radial thermal response will also provide confirmation of the role of pile-soil

interface stresses due to radial thermal expansion of energy piles on their ultimate capacity, which has been proposed as a possible mechanism contributing to the side shear resistance of centrifuge-scale energy piles in compacted silt along with changes in effective stress in unsaturated soils associated with thermally induced drying (McCartney and Rosenberg, 2011; Goode and McCartney, 2015). Preliminary numerical and analytical studies using cavity expansion analyses by Olgun et al. (2014) and Zhou et al. (2016) indicate that no significant changes in pile-soil interface stresses are expected from the radial thermal expansion of the pile. However, these studies have not been validated against field scale studies.

The main objective of this paper is to explore the axial and radial thermal responses of a field scale energy pile at a similar depth during both monotonic and cyclic changes in pile temperatures. The energy pile, previously studied by Wang et al. (2015) and Singh et al. (2015), was subjected to four operational temperature modes, including monotonic heating, monotonic cooling, intermittent cooling with natural ground thermal recharging, and intermittent cooling with forced ground thermal recharging. Different pile temperatures were observed to lead to different magnitudes of axial and radial thermal loads in the pile and at the pile-soil interface.

Ground Conditions

The soil deposit at the pile test site is part of the Brighton Group Sediments, which is an important geological unit of Melbourne because of its extensive surface coverage of the south-eastern suburbs of the city. The Brighton Group consists of two major formations: the Red Bluff Sands and the underlying Black Rock Sandstone. The Red Bluff Sands are commonly encountered in outcrop and include clays, sandy clays, clayey sands, sands and occasionally silts. The stratigraphy of the Red Bluff Sands frequently shows a surface layer of clay or clayey

sand with a decrease in clay content with depth leading into silty sands and sands. The ground conditions at the test site are summarized in Table 1.At the test site, the soil profile consists of dense sand below a depth of 2.5 m. There is no groundwater table present at the test site within the depth of the pile (Wang et al., 2015; Singh et al., 2015), and the soil is unsaturated.

Energy Pile Details and Experimental Procedures

A schematic of the instrumented energy pile used in this study is shown in Fig. 1. The 0.6 m diameter bored pile was installed to a depth of 16.1 m, and included a two-level Osterberg Cell (O-Cell) load testing system. Three high-density polyethylene (HDPE) pipe closed loop heat exchangers in a "U" configuration (U-loops), having outer and inner pipe diameters of 25 mm and 20 mm, respectively, were attached to the inside of the reinforcing cage of the pile. The pipes were installed 50 mm from the edge of the pile and up to a depth of 14.2 m. The horizontal spacing between the loops was approximately 175 mm. The head of the pile is free to move during heating and cooling, so the effects of the head restraint are assumed to be negligible (Knellwolf et al., 2011; Chen and McCartney, 2016). Further, the toe of the pile is assumed to be free to move downward due to the presence of the O-Cells. Accordingly, the upper portion of the energy pile is assumed to only be restrained by the mobilized side shear forces, and the end restraint boundary conditions on the axial thermal response of the energy pile can be neglected.

The pile was specifically designed to study the changes in pile shaft capacity after thermal loading (Wang et al., 2015), and thus is different from a conventional energy pile (i.e, it included two O-cells). The two O-Cells were located at depths of approximately 10 m and 14 m, dividing the pile into three sections: a 10 m-long upper section, a 4 m-long middle section,

158 and a lower 1 m-long section. Only the upper pile section is considered for analysis in this
159 paper. The axial and radial thermal responses are assessed at depths of 5.4 m and 6.4 m,
160 respectively. These depths are within the same soil layer and are close enough that the thermo-
161 mechanical response of the energy pile is assumed to be the same. As indicated earlier, the
162 focus of this paper is on a comparison of the magnitudes of axial and radial thermal strains and
163 stresses at a single depth, which are a function of the restraint provided by the surrounding
164 subsurface on the energy pile. This is a different analysis from previous studies that focused on
165 evaluation of the shapes of the thermal strain and stress profiles as a function of depth to
166 evaluate soil-structure interaction mechanisms (Bourne-Webb et al., 2009; Murphy et al., 2015;
167 Murphy and McCartney, 2015; McCartney and Murphy, 2017). It is possible that the
168 comparison between the axial and radial thermal strains and stresses may be different near the
169 ends of the piles, which is one reason that the particular location between 5.4 m and 6.4 m was
170 selected for this evaluation.
171
172 Embedment and sister bar vibrating wire strain gauges were installed at different depths in the
173 pile, shown in Fig. 1. Type K thermocouples recorded the inlet and outlet water temperatures
174 at the pile head. The thermocouple data were logged using a Pico Technology's USB-TC08
175 data logger. Data from strain gauges were recorded using DataTaker's DT80G and CEM20
176 data loggers. The concrete mix used in the pile was supplied by Holcim Australia Pty. Ltd. It
177 consisted of 7 mm aggregates, cement, and fly ash with a water to cement ratio of 0.45. The
178 compressive strength of the pile concrete was 40.9 MPa and 65.6 MPa after 35 and 210 days,
179 respectively (Wang, 2017). The cooling and heating units were connected to the pile inlet and
180 outlet using insulated HDPE pipes, with an approximate length of 15 m. The pile head and the
181 ground surface were not restrained and were exposed to the atmosphere.
182

Four sets of experiments were carried out in this study in the following sequence: 1) monotonic heating for twenty-four hours (24H mode) with a water flow rate of 10 liters per minute (LPM) and a target inlet water temperature of 45 °C. (note: the inlet water temperature increased gradually throughout the test and was not constant); 2) monotonic cooling for twenty-four hours (24C mode) with a water flow rate of 15 LPM, and a target inlet water temperature of 5 °C; 3) cooling for sixteen hours followed by eight hours rest (16N mode), daily, simulating intermittent operation with natural ground thermal recovery with a flow rate of 15 LPM and an inlet water temperature of 5°C; and 4) cooling for sixteen hours followed by heating for eight hours (16F mode), simulating daily intermittent operation with scheduled forced ground thermal recovery for a solar-hybrid system with a flow rate of 15 LPM and an inlet water temperature ranging from 7 to 16 °C in the cooling cycle, and a flow rate of 13.5 LPM and an inlet water temperature ranging from 30 to 55 °C during the heating cycle. The inlet water temperatures for all experiments are shown in Fig. 2. The water temperatures from each cycle affected the other cycle throughout the experiments when switching between cooling and heating cycles in the 16F mode. This variation in temperature is expected in practice in geothermal systems with alternating heating/cooling operations (Dai et al., 2015). The fluid flow in the heat exchange tubing with the pile was stopped multiple times to control the inlet water temperatures before re-establishing flow. there was an operational failure of the cooling unit for approximately 16 hours on Day 21 in the 24C mode, and an operational failure of the cooling unit for 15 hours on Day 16 in the 16F mode, but these did not have major effects on the interpretation of the test results. After the experiments resumed, the magnitudes of the pile temperatures (Fig. 4) and thermal strains (Fig. 5) in the 24C and 16F modes stabilized to the magnitudes recorded before the operational failure, hence confirming the repeatability of the tests. A summary of the experiments is given in Table 2. Up to twenty-four days of data are

considered for all modes for the sake of brevity in the analysis. The pile temperatures and thermal strains recovered to near initial conditions after completion of the experiments.

Mechanisms of Thermal Response

The mechanisms of axial thermal response of energy piles has been widely evaluated using experimental results from previous field studies (Bourne-Webb et al., 2009; Amatya et al., 2012; Bourne-Webb et al., 2013) while only a limited evaluation of the mechanism of radial thermal response has been performed (Olgun et al., 2014). As indicated earlier, the upper portion of the energy pile evaluated in this study is assumed to be restrained by the mobilized side shear forces only while the effect of the end restraint boundary conditions on the axial thermal response can be neglected owing to the unconfined condition at the ground surface and the presence of the O-Cell at the toe (i.e., the pile can be treated as a floating pile with no end restraints). Based on these assumptions, a mechanism of axial and radial thermal responses of the upper pile section is adopted for analysis of results as shown in Fig. 3. The mechanisms considered herein are based on the expansive and contractive forces in the pile and the resulting reaction forces at the pile-soil interface and do not consider the thermo-hydro-mechanical processes in the surrounding soil. The sign convention in this study is similar to that in engineering mechanics, where positive and negative stresses correspond to tension and compression, respectively.

The thermally induced expansive and contractive forces developed in the energy pile are opposed by the side shear restraint provided by the surrounding subsurface, and as a result, additional thermal stresses are developed in the pile and at the pile soil interface. During heating, the pile expands axially outwards from the null point (the point in the pile where thermally

induced displacement is zero). The reaction forces or mobilized axial side shear stresses act in the opposite direction of expansion i.e. downward friction develops above the null point and upward friction develops below the null point. Compressive thermal stresses are developed in the pile due to the restraint provided by the surrounding soil (Fig. 3a). Axial pile contraction due to cooling develops opposite effects to that of heating, i.e. the pile contracts axially towards the null point, the mobilized axial side shear stresses act upwards above the null point and downwards below the null point, and expansive thermal stresses are developed in the pile (Fig. 3b). No axial thermal stresses develop at the ends of the pile for both cooling and heating due to the lack of end restraint boundary conditions.

Lateral expansion from heating, which is assumed to occur radially outwards from the center of the pile, leads to the development of compressive radial stresses in the pile due to the restraint provided by the surrounding subsurface. The reactive forces from the surrounding soil or the radial pile-soil contact stresses are equal and opposite to that induced by pile radial expansion to maintain radial stress equilibrium (Fig. 3c). Lateral contraction from cooling develops radial thermal responses opposite to that of heating (Fig. 3d). The following results and discussions are based on these thermal response mechanisms.

Results and Discussions

Pile Temperatures

The pile temperatures at depths of 5.4 m and 6.4 m are shown in Figs. 4a and 4b, respectively, while the changes in pile temperature, ΔT, with respect to the initial undisturbed temperature of the pile are shown in Figs. 4c and 4d, respectively. The initial pile temperatures at these two

depths range between 15.8 and 17.5°C, which are similar to the initial temperatures of the soil at these depths below ground surface (Singh et al., 2015; Yu et al., 2015).

The pile temperatures at both depths show similar trends and magnitudes, with a difference of less than 0.5 °C. The ratio of pile temperatures at a depth of 5.4 m to a depth of 6.4 m is shown in Fig. 4e, and is close to one. This confirms that the pile temperatures at these two locations are similar. An almost constant pile temperature of 6 °C is obtained in the 24C mode. The pile temperatures in the 24H mode gradually increased to 40 °C due to the gradual increase of the inlet water temperatures shown in Fig. 2. The pile temperatures cycled between 6 and 9 °C in the 16N mode and between 10 and 33 °C in the 16F mode.

Active heating during thermal recharging in the 16F mode developed much higher pile temperatures compared to the 16N mode. The pile temperatures at the end of heating in the 16F mode dropped slightly below the undisturbed pile temperatures; hence, the ΔT magnitudes were also slightly negative at the end of heating. This led to difficulties in estimating the transient mobilized thermal expansion coefficients and thermal stresses of the 16F mode, as discussed in the following sections.

Pile Thermal Strains

The transient axial and radial thermal strains induced in the concrete, ε_T, are shown in Figures 5a and 5b, respectively, for the four experiments. The thermal strains measured using the vibrating wire strain gauges were corrected for temperature effects as follows:

$$\varepsilon_T = (f_i^2 - f_o^2)GB + (T_i - T_o)\alpha_s \quad (1)$$

where f_i is the resonant frequency of the strain gauges at time i, f_o is the reference resonant frequency of the strain gauges, GB is the calibration factor (G is gauge factor, and B is batch factor) of the strain gauges, T_i is the temperature of the strain gauges at time i, T_o is the reference temperature of the strain gauges, α_s is the coefficient of linear thermal expansion of steel wire in the strain gauges (12 με /°C). The value of f_o was selected at the beginning of each experiment and thus removes the effects of any strains due to the self-weight of the pile or curing of the concrete.

Both the axial and radial thermal strains closely follow the trends in monotonic and cyclic pile temperature shown in Fig. 4. Similar to the magnitudes of ΔT during the 16F mode in Fig. 4, the thermal strains in the 16F mode were slightly negative at end of heating indicating expansion of the pile. Unlike the pile temperatures, the magnitudes of the axial and radial thermal strains are different. Compared to the magnitudes of the axial thermal strains, the radial thermal strains are up to 40% higher for all modes, indicating that the energy pile was more restrained in the axial direction than the radial direction at this depth.

The relationships between the thermal strains and the change in pile temperature ΔT are shown in Fig. 5c. The thermal strains and ΔT data were extracted at Day 20 of each experiment (average values are taken for the 16F and 16N modes). The magnitude of axial thermal strains for a given change in pile temperature is lower (8.55 με/°C) than the radial thermal strains (11.71 με/°C), confirming that the side shear stresses provide more restraint to the axial thermal strains than the surrounding subsurface to radial thermal strains. This led to the development of larger axial thermal stresses than radial thermal stresses in the pile, which is discussed later in the paper. The radial thermal strains reflect lower restraint to thermal expansion/contraction

307 compared to the axial thermal strains, which may be because the ratio of the pile diameter (D)
308 to the thermally active pile length (L) is small in magnitude (i.e., D/L = 0.04).
309
310 The ratios of axial to radial thermal strains for the four experiments are shown in Fig. 5d. The
311 16F mode experiment, as shown in Figs. 4c and 4d and Figs. 5a and 5b, faced frequent reversals
312 (i.e., cycling between negative and positive values). As a result, unrealistically high ratios of
313 axial to radial thermal strains are obtained in this experiment when compared to the other trhee
314 experiments, mainly when the thermal strains are close to zero. Further, unrealistically high
315 mobilized thermal expansion coefficinets, $\alpha_{mobilized}$, (discussed later) are also obtained when
316 the thermal strain and ΔT values are close to zero, which led to difficulties in estimating the
317 transient thermal stresses in a pile experiencing temperature reversals similar to the
318 observations of Murphy and McCartney (2015). The issues of unrealistic ratios of thermal
319 strains and thermal expansion coefficients faced by frequent temperature reversals in the 16F
320 mode were addressed by translating the ΔT and thermal strain diagrams (Figs. 4c and d, and
321 Figs. 5a and b, respectively) vertically upwards by an amount equal to the minimum values on
322 the respective diagram. The minimum axial thermal strain and ΔT values were -61.93 με
323 and -7.7°C, respectively, and the minimum radial thermal strain and ΔT values were -97.55 με
324 and -7.5°C, respectively. This translation caused the thermal strain and ΔT magnitudes to
325 become positive and the issue of temperature reversals was thus eliminated.
326
327 The ratios of axial to radial thermal strains in Fig. 5d indicate a stable response with operating
328 time in the different experiments, indicating that the thermally induced volumetric
329 expansion/contraction of the pile at the considered location remains almost constant. The strain
330 ratio for the 24H, 24C, and the 16N modes are within the same band of magnitudes (i.e.,
331 between 0.7 and 0.77), indicating that monotonic and very low range cyclic temperatures leads

to similar volumetric expansions/contractions of the energy pile. The relatively large range of cyclic temperatures in the 16F mode led to larger fluctuations in the thermal strain ratio compared to other modes. However, the trend in the strain ratio in the 16F mode is also stable, indicating that the volumetric expansion/contraction for large cyclic temperature fluctuations is stable as well.

Pile-Soil Radial Contact Stresses

The pile-soil radial contact stresses, σ_n, resulting from the radial thermal expansion/contraction of the pile were estimated using a cavity expansion analysis, given as follows:

$$\sigma_n = \frac{E_s}{1+v_s}\frac{\Delta r}{r} \quad (2)$$

where E_s and v_s are the Young's modulus and Poisson's ratio of the surrounding dense sand (assumed to be 60 MPa and 0.3, respectively, based on typical values for dense sand), r is the pile radius, and Δr is the thermally induced radial displacement of the pile. This displacement acts against the restraint provided by the surrounding soil and affects the soil-pile radial interface stress. The value of Δr/r is assumed to be equal to the radial strain measured in the experiment for a given change in temperature. Laboratory studies conducted on sand samples collected from the site have shown that the shear strength of the dense sand is not affected by temperature variations (Barry-Macaulay, 2013). Other studies have also indicated that the effect of temperature variations on the shear strength of sand is insignificant (Donna et al. 2015; Yavari et al., 2016b). Also, the thermally induced change in pile radius, Δr, is relatively small compared to the initial pile radius. Hence, this simple model assuming a constant stiffness was deemed to be useful for analyzing the pile-soil radial contact stresses.

The pile-soil radial contact stresses of all the studied modes are compared in Fig. 6a. The contact stresses stabilize with time, indicating that there is no degradation in the pile-soil contact stresses for the monotonic and cyclic temperatures studied. The numerical study reported by Olgun et al. (2014) observed that the contact stresses between the pile and soil due to radial thermal expansion during monotonic heating are small in magnitude, even for large differences in thermal expansion coefficients for the two materials. A radial contact stress of up to 15 kPa was reported in their study for a range of typical soil moduli and temperature change up to 10°C, while a maximum value of up to 12 kPa is observed in the present study for a change in temperature of 22.5 °C. The slope of the relationship between the contact stresses and the change in pile temperatures, shown in Fig. 6b, is 0.54 kPa/°C. This small magnitude of the slope indicates that the radial contact stresses of the pile-soil interface will likely be negligible for the commonly encountered operating temperatures in energy piles and the typical construction procedures used for cast-in place concrete energy piles.

Thermal Expansion Coefficients and Thermal Stresses

A comparison of the axial and radial thermal expansion coefficients of the concrete restrained by the interaction between the pile and the soil ($\alpha_{mobilized}$ coefficients) is done for all the modes. The transient axial and radial $\alpha_{mobilized}$ coefficients are calculated by dividing the thermal strains, ε_T, by the respective change in pile temperatures, ΔT.

The transient variations in the $\alpha_{mobilized}$ coefficients for the 24C, 24H, 16N, and 16F modes are shown in Figs. 7a to 7d, respectively. As discussed earlier, the thermal strains and ΔT

magnitudes in the 16F mode were translated to positive magnitudes to eliminate issues of temperature reversals. The lower magnitude of the axial $\alpha_{mobilized}$ coefficients than the radial $\alpha_{mobilized}$ coefficients for all four experiments reflect that the axial expansion/contraction of the pile is more restrained, which again confirms that the energy pile is more restrained axially. This leads to differences between the axial and radial thermal stresses developed in the pile, shown in Fig. 8. The radial and axial $\alpha_{mobilized}$ coefficients ranged between 10 and 13.8 με/°C and 6 and 12.2 με /°C, respectively, for all four experiments. There are slight differences in the $\alpha_{mobilized}$ coefficients between the different modes due to differences in ΔT, and hence differences in the thermal effects on pile expansion/contraction. The magnitudes of the radial $\alpha_{mobilized}$ coefficients are closer to the magnitudes of the free (unrestrained) thermal expansion coefficient of the concrete (α_{free} coefficients), indicating that the energy pile expands/contracts almost freely in the radial direction with minimal restriction from the surrounding soil. This may be due to the particular construction effects associated with drilled shaft foundations.

The thermal axial and radial stresses developed in the pile were estimated as follows (Amatya et al. 2012; Murphy et al., 2015; Caulk et al., 2016):

$$\sigma_T = E_p(\alpha_{mobilized} - \alpha_{free})\Delta T \quad (3)$$

where E_p is the Young's modulus of the concrete (taken as 30 GPa), $\alpha_{mobilized}$ is the thermal expansion coefficient of the concrete restrained by the pile-soil interaction, α_{free} is the free (unrestrained) thermal expansion coefficient of the concrete, and ΔT is the change in concrete temperature. An average value of α_{free} = 12 με /°C was considered and was slightly adjusted within ± 1 με /°C for different operating modes to confirm that the magnitudes of the radial

406 thermal stresses developed in the pile are equal to the pile-soil radial contact stresses (i.e. σ_n =
407 σ_T for radial stress equilibrium). The coefficient of linear thermal expansion of concrete
408 depends on the aggregate mineralogy of the mix and has been reported to range from 9 με/°C
409 to 14.5 με/°C while that of steel reinforcement has been reported to range from 11.9 με/°C to
410 13 με/°C (Stewart and McCartney, 2014). An average value of α_{free} = 12 με /°C has been
411 used for analysing some field scale energy piles (Murphy and McCartney, 2012; Murphy et al.
412 2015; McCartney et al. 2015; Caulk et al., 2016) as differential thermal strains are not expected
413 between the concrete and the steel reinforcements. The sign convention used in this study is
414 similar to that in engineering mechanics, where negative stresses correspond to compression,
415 so the values of α have positive values.
416
417 The variations of axial and radial thermal stresses are shown in Figs. 8a and 8b, respectively.
418 Heating leads to the development of compressive stresses which are considered as negative
419 while cooling leads to the development of tensile stresses which are considered as positive. The
420 thermal stresses observed in all the experiments are much lower than the compressive strength
421 of the concrete, which are 40.9 and 65.6 MPa after 35 and 210 days, respectively. Hence, no
422 temperature-induced structural damage to the pile is expected for the range of temperatures
423 studied herein.
424
425 Since the thermal strains and ΔT in the 16F mode were translated to positive magnitudes when
426 calculating the thermal expansion coefficients, the radial thermal stresses of the 16F mode were
427 back-analyzed to estimate the magnitudes of the pile-soil contact stresses needed to maintain
428 radial thermal stress equilibrium (Fig. 8b). The offset is 4.5 kPa. The axial thermal stresses of
429 the 16F mode in Fig. 8a were however not back-analyzed as there was no reference value
430 available. The axial thermal strains in the 16F mode at end of the heating cycle do not exceed

that of the 24H mode (Fig. 5a). The thermal stresses in the 16F mode at the end of the heating cycle are thus expected to be approximately equal to that of the 24H mode.

The radial thermal stresses are very small in magnitude when compared to the axial thermal stresses in all four experiments. This is due to the differences in restrictions of the thermal strains and mobilized thermal coefficients discussed in Figs. 5 and 7. The magnitude of the radial thermal stresses against change in pile temperatures is thus very small (-0.54 kPa/°C) compared to the axial thermal stresses (-106.34 kPa/°C), shown in Fig. 8c. Amatya et al. (2012) assessed the axial thermal stresses against change in pile temperatures of the Lausanne energy pile (Laloui et al., 2006) and the Lambeth College heat sink pile (Bourne-Webb et al., 2009) without head loads and reported maximum values of -104 kPa/°C for the Lausanne case and -192 kPa/°C for the Lambeth College case. Thus, the current axial thermal stresses against change in pile temperatures are within the range reported in literature for similar head load conditions.

The highest axial and radial thermal stresses in Figs. 8a and b are approximately 3 MPa and 12 kPa, respectively. Large differences in axial and radial stresses for heating and cooling were also reported by Gawecka et al. (2017). They numerically back analyzed the Lambeth College energy pile test (Bourne-Webb et al. 2009) and performed an explorative study considering the fully coupled thermo-hydro-mechanical response of the London Clay. They reported axial thermal stresses ranging from approximately 5 to 0.5 MPa from the head to the toe, respectively, of a 23 m long pile with a 1200 kN head load. The radial stresses were approximately 10 kPa to 30 kPa from the head to the toe of the pile, respectively. The axial stresses reduced from head to toe of the pile, while the radial stresses were found to increase with depth and were largest close to the base, probably due to end effects. In another numerical study on the heating

effects of an energy pile in clay and without head loads, Ozudogru et al. (2015) also reported that the change in radial stresses with temperature was small in magnitude and in the order of a few kilopascals compared to the change in axial thermal stresses.

Mimouni and Laloui (2015) assessed the heating effects on axial and radial thermal strains in one of four field scale bored energy piles (diameter of 0.9 m and length of 28 m) installed under a water retention tank. The radial strains were compared at 9 m depth (in soft alluvial clays and loose sandy gravelly moraine) and at 19 m depth (in stiff bottom moraine and sandstone). The observed radial thermal strains were found to be much lower than the free radial thermal expansion of the pile, indicating that the soil formation at their site provided higher restrictions to radial thermal responses than the soil formation in the current study. The radial thermal strains in stiff soils at 19 m depth were found to be completely restricted to thermal expansion than the radial strains in softer soils at 9 m depth, indicating that stiffer soils and possibly higher depths developed larger radial thermal stresses. Gawecka et al. (2017) also found in their numerical study that radial stresses increased with depth and were largest near the toe.

Mimouni and Laloui (2015) monitored axial strains at 2 m intervals in an energy pile and were able to compare the restrictions to thermal expansion in axial thermal strains at different depths. The highest axial strain restriction was at a depth of 24 m closer to the toe of the pile in stiff sandstone. Since the radial strains at a depth of 19 m were completely restricted to thermal expansion, they were able to assess the effects of blocked radial strains that could have caused large restrictions of the axial thermal strains at a depth of 24 m. The current study however assesses the axial and radial thermal responses near the mid-depth of the upper pile section only. The axial and radial thermal responses at other locations was not possible for comparative

480 purposes, the effects of any blocked radial strains on the axial strain restrictions was not
481 assessed.
482
483 The results in Fig. 8 indicate that the axial thermal stresses are more dominant than radial
484 thermal stresses in developing additional thermal loads in energy piles (i.e. thermally induced
485 changes in the piles side, base and head resistances). Load transfer analysis models for
486 predicting the thermo-mechanical behaviour of energy piles have also suggested that radial
487 thermal effects can be ignored in comparison to axial thermal effects. Knellwolf et al. (2011)
488 conducted a load transfer analysis by neglecting the radial displacements and their mechanical
489 interactions with the soil as these were considered small with regards to axial displacements.
490 They validated their method with the Lambeth College and Lausanne field scale energy piles
491 and found that their method was able to reproduce good axial thermo-mechanical behavior. A
492 detailed parametric load transfer analysis of energy piles was recently conducted by Chen and
493 McCartney (2016) to validate and predict the axial thermal strains, stresses and displacements
494 of a field energy pile and several centrifuge-scale energy piles. They also concluded that the
495 effects of radial thermal strain was relatively small and can be neglected in load transfer
496 analysis. The results of the axial and radial thermal responses of the current study confirms the
497 recommendations of load transfer analysis models and could also help strengthen such
498 predictive models for designing field scale energy piles. The relationships between the thermal
499 loads and change in pile temperatures could be useful for estimating expected thermal loads
500 during designing energy pile systems for similar soil conditions and commonly expected range
501 of operational pile temperatures.
502
503 ***Temperature-Dependent Thermal Response of the Pile***
504

505 Plots of the axial and radial thermal strain variations versus the pile temperature change, ΔT,
506 up to Day 20 for each of the four experiments are shown in Fig. 9. The results are presented at
507 four-day intervals for better clarity of the temperature dependent response of the pile. The
508 trends observed again confirm that the axial thermal strains are more restrained than the radial
509 thermal strains. Between Days 1 – 8, a ratcheting behavior of the axial and radial thermal strains
510 with irreversible paths is observed for the 16F mode (Figs. 9a and 9c, respectively) and the
511 16N mode (Fig. 9e). Radial thermal strains show less ratcheting behavior than axial thermal
512 strains due to the lower restraint to thermal expansion/contraction. Between Days 12 – 20, the
513 thermal strains follow reversible cyclic paths with linear hysteresis loops between stable ΔT for
514 both the cyclic modes (Figs. 9b, 9d and 9f). This observation indicates that the initial ratcheting
515 behavior results from unstable pile temperatures and not from pile or soil settlements. Pile
516 temperatures are initially unstable due to high initial heat dissipation in the sand resulting from
517 the high gradients associated with the sudden temperature changes.
518
519 The thermal strains of the 24C and 24H modes are shown in Figs. 9g and 9h, respectively. The
520 axial and radial thermal strains change linearly with monotonic ΔT for both modes. There are
521 larger changes in thermal strains as well as in ΔT on Day 1 for both of these experiments,
522 although the rate of change in the thermal strain decreases between Days 4 – 20. The slight
523 differences in thermal strains between Days 4 – 20 for both experiments (particularly for the
524 24H mode) are small in magnitude compared to the changes observed the beginning of the
525 experiments. The large changes in thermal strains at the beginning of the experiments for the
526 monotonic modes are likely due to unstable pile temperatures and are not expected to be due
527 to not due to pile or soil settlements.
528

529 The stable responses of the axial and radial thermal strains towards the end of experiments for
530 both monotonic and cyclic temperatures indicate that the shaft resistance is not significantly
531 affected, relative settlements between the pile and the soil do not occur from thermally induced
532 deformations of the dense sand, and no significant lateral load is transferred to axial loads as a
533 result of changes in the pile-soil contact stresses. There was also no degradation in the shaft
534 capacity reported from monotonic heating on this pile, which was assessed by partially
535 translating the upper section of the pile upwards using the internal O-Cells (Wang et al., 2015).
536
537 The surrounding dense sand provides a relatively high resistance to thermal deformations of
538 the pile and the soil at the current site. Numerical studies conducted by Saggu and Chakraborty
539 (2015) showed that energy pile settlements in dense sand are much lower than in loose sand
540 due to differences in the shaft friction. A comparative assessment of the Lambeth College and
541 Lausanne field scale energy piles, installed in mostly stiff and soft clays, respectively, has
542 shown that the stiffer London clay imposed a higher resistance to deformation at the pile-soil
543 interface (Amatya et al., 2012). Another reason for the stable responses of the thermal strains
544 towards the end of experiments is that there were no head loads on the pile or end restraints in
545 the present study. According to some physical model studies with thermal cycles on energy
546 piles (Kalantidou et al., 2012; Stewart and McCartney, 2013, Yavari et al., 2014, 2016a; Wang
547 et al., 2016), thermally induced settlement is reversible for pile head loads corresponding to as
548 low as 20% of the pile ultimate resistance, and becomes irreversible for higher pile loads,
549 particularly for loads closer to the ultimate pile resistance. However, the soil type plays an
550 important role in the thermal response of the pile, and the dense sand at the current site likely
551 contributed to the relatively high resistance to axial thermal deformations.
552
553 **Conclusions**

554

555 This study investigated the axial and radial thermal response of a field scale energy pile under
556 monotonic and cyclic temperature changes. The radial thermal strains are found to be less
557 restrained to thermal expansion/contraction and are approximately 40% greater than the axial
558 thermal strains for all experimental conditions investigated. The radial thermal strains are close
559 to those corresponding to free thermal expansion/contraction, indicating that the soil provides
560 minimal resistance to radial thermal expansion/contraction. Accordingly, the magnitudes of the
561 radial thermal stresses developed in the pile are much lower than the axial thermal stresses, and
562 may not play a major role in soil-structure interaction for the typical setting of cast-in-place
563 concrete energy piles. The pile-soil contact stresses estimated using cavity expansion analysis
564 are at most 12 kPa and are negligible for the commonly encountered operating temperatures in
565 energy piles. Unstable responses of the axial and radial thermal strains were observed at the
566 beginning of the experiments (i.e., a ratcheting response under cyclic temperatures and large
567 changes in thermal strains under monotonic temperatures), but these responses stabilized with
568 operating time as the pile temperatures stabilized. The stable thermal responses of the pile after
569 several cycles indicate that no significant changes in the side friction, pile-soil contact stresses,
570 and shear strength are expected for energy piles in a similar setting to that investigated in this
571 (drilled shafts in dense sand). Finally, the results reported herein are only representative of one
572 section of an energy pile (the upper part) in unrestrained conditions at the heat and toe and
573 without a mechanical load applied to the head, so further studies are warranted on conventional
574 energy piles under actual loading and end restraint conditions to capture the complete
575 distribution of axial and radial thermal strains along the length of the pile.

576

577 **Acknowledgements**

578

579 The geothermal energy pile installation was funded by the Victorian Government Sustainability
580 Fund (2009 – 2012), Vibropile Pty. Ltd., Golder Associates Pty. Ltd., and GeoExchange
581 Australia Pty. Ltd. (Project No. 4678). This research project is supported under the Australian
582 Research Council's Linkage Projects funding scheme (project number LP120200613). The
583 authors also acknowledge the Australian Government Research Training Program Scholarship
584 provided to the first author. The last author was supported by US National Science Foundation
585 grant CMMI-0928159. The support of all the sponsors is gratefully acknowledged.
586

587 **References**

588

589 Akrouch, G., Sánchez, M. and Briaud, J-L. (2014). "Thermo-mechanical behavior of energy
590 piles in high plasticity clays." *Acta Geotechnica*, 9(3), 399-412.
591 Amatya, B. L., Soga, K., Bourne-Webb, P. J., Amis, T. and Laloui, L. (2012). "Thermo-
592 mechanical behaviour of energy piles." *Géotechnique*, 62(6), 503-519.
593 Barry-Macaulay, D. (2013). "An investigation on the thermal and thermo-mechanical
594 behaviour of soils." Master of Engineering Thesis, Monash University, Melbourne,
595 Australia.
596 Barry-Macaulay, D., Bouazza, A., Singh, R. M., Wang, B. and Ranjith, P. G. (2013). "Thermal
597 conductivity of soils and rocks from the Melbourne (Australia) region." *Engineering*
598 *Geology*, 164, 131-138.
599 Bourne-Webb, P. J., Amatya, B., Soga, K., Amis, T., Davidson, C. and Payne, P. (2009).
600 "Energy pile test at Lambeth College, London: geotechnical and thermodynamic
601 aspects of pile response to heat cycles." *Géotechnique*, 59(3), 237-248.

602 Bourne-Webb, P. J., Amatya, B., and Soga, K. (2013). "A framework for understanding energy
603 pile behaviour." *Proceedings of the Institution of Civil Engineers - Geotechnical*
604 *Engineering*, 166(2), 170-177.
605 Brandl, H. (2006). "Energy foundations and other thermo-active ground structures."
606 *Géotechnique*, 56(2), 81-122.
607 Bouazza, A., Singh, R.M., Wang, B., Barry-Macaulay, D., Haberfield, C., Chapman, G.,
608 Baycan, S. and Carden, Y., (2011). "Harnessing on site renewable energy through pile
609 foundations." *Australian Geomechanics*, 46(4), 79-89.
610 Caulk, R., Ghazanfari, E., and McCartney, J.S. (2016). "Parameterization of a calibrated
611 geothermal energy pile model." *Geomechanics for Energy and the Environment*, 5(3),
612 1-15.
613 Chen, D. and McCartney, J.S. (2016). "Parameters for load transfer analysis of energy piles in
614 uniform nonplastic soils." *International Journal of Geomechanics*, 17 (7),
615 10.1061/(ASCE)GM.1943-5622.0000873, 04016159-1-17.
616 Di Donna, A., Ferrari, A., and Laloui, L. (2015). "Experimental investigations of the soil–
617 concrete interface: physical mechanisms, cyclic mobilization, and behaviour at
618 different temperatures." *Canadian Geotechnical Journal*, 53(4), 659-672.
619 Dai, L., Li, S., DuanMu, L., Li, X., Shang, Y., and Dong, M., (2015). "Experimental
620 performance analysis of a solar assisted ground source heat pump system under
621 different heating operation modes." *Applied Thermal Engineering*, 75, 325-333.
622 De Moel, M., Bach, P. M., Bouazza, A., Singh, R. M., and Sun, J. O. (2010). "Technological
623 advances and applications of geothermal energy pile foundations and their feasibility
624 in Australia." *Renewable and Sustainable Energy Reviews*, 14(9), 2683-2696.
625 Faizal, M., Bouazza, A. and Singh, R. M. (2016). "An experimental investigation of the
626 influence of intermittent and continuous operating modes on the thermal behaviour of

627 a full scale geothermal energy pile." *Geomechanics for Energy and the Environment*,
628 8, 8-29.
629 Gawecka, K. A., Taborda, D. M. G., Potts, D. M., Cui, W., Zdravković, L., and Kasri, M. S. H.
630 (2017). "Numerical modelling of thermo-active piles in London Clay." *Proceedings of*
631 *the Institution of Civil Engineers - Geotechnical Engineering*, 170(3), 201-219.
632 Goode, J. C. and McCartney, J. S. (2015). "Centrifuge modeling of end-restraint effects in
633 energy foundations." *Journal of Geotechnical and Geoenvironmental Engineering*,
634 10.1061/(ASCE)GT.1943-5606.0001333, 04015034-1-13.
635 Jalaluddin and Miyara, A. (2012). "Thermal performance investigation of several types of
636 vertical ground heat exchangers with different operation mode." *Applied Thermal*
637 *Engineering*, 33–34, 167-174.
638 Kalantidou, A., Tang, A. M., Pereira, J-M. and Hassen, G. (2012). "Preliminary study on the
639 mechanical behaviour of heat exchanger pile in physical model." *Géotechnique*, 62(11),
640 1047-1051.
641 Knellwolf, C., Peron, H., and Laloui, L. (2011). "Geotechnical analysis of heat exchanger piles."
642 *Journal of Geotechnical and Geoenvironmental Engineering*, 130 (10),
643 10.1061/(ASCE)GT.1943-5606.0000513, 890–902.
644 Laloui, L., Nuth, M. and Vulliet, L. (2006). "Experimental and numerical investigations of the
645 behaviour of a heat exchanger pile." *International Journal for Numerical and*
646 *Analytical Methods in Geomechanics*, 30(8), 763-781.
647 McCartney, J.S. and Murphy, K.D. (2012). "Strain distributions in full-scale energy
648 foundations." *DFI Journal: The Journal of the Deep Foundations Institute*, 6(2), 26-38.
649 McCartney, J.S. and Murphy, K.D. (2017). "Investigation of potential dragdown/uplift effects
650 on energy piles." *Geomechanics for Energy and the Environment*, 10, 21-28.

McCartney, J.S. and Rosenberg, J.E. (2011). “Impact of heat exchange on side shear in thermo-active Foundations.” *Geo-Frontiers 2011*, ASCE, Texas, United States, 488-498.

McCartney, J.S., Murphy, K.D., and Henry, K.S. (2015). “Response of an energy foundation to temperature fluctuations.” *IFCEE*, ASCE, San Antonio, Texas, United States, 1691–1700.

Mimouni, T. (2014). “Thermomechanical characterization of energy geostructures with emphasis on energy piles.” PhD thesis, École Polytechnique Fédérale de Lausanne, Lausanne, Switzerland.

Mimouni, T. and Laloui, L. (2015). “Behaviour of a group of energy piles.” *Canadian Geotechnical Journal*, 52(12), 1913-1929.

Murphy, K.D. and McCartney, J. S. (2015). “Seasonal response of energy foundations during building operation.” *Geotechnical and Geological Engineering*, 33(2), 343-356.

Murphy, K. D., McCartney, J. S., and Henry, K. S. (2015). “Evaluation of thermo-mechanical and thermal behavior of full-scale energy foundations.” *Acta Geotechnica,* 10(2), 179-195.

Ng, C. W. W., Gunawan, A., Shi, C., Ma, Q. J. and Liu, H. L. (2016). “Centrifuge modelling of displacement and replacement energy piles constructed in saturated sand: a comparative study.” *Géotechnique Letters*, 6(1), 34-38.

Ng, C. W. W., Shi, C., Gunawan, A. and Laloui, L. (2014a). “Centrifuge modelling of energy piles subjected to heating and cooling cycles in clay.” *Géotechnique Letters*, 4(4), 310-316.

Ng, C. W.W., Shi, C., Gunawan, A., Laloui, L. and Liu, H. L. (2014b). “Centrifuge modelling of heating effects on energy pile performance in saturated sand.” *Canadian Geotechnical Journal*, 52(8), 1045-1057.

675 Olgun, C.G., Ozudogru, T. Y. and Arson, C. F. (2014). "Thermo-mechanical radial expansion
676 of heat exchanger piles and possible effects on contact pressures at pile–soil interface."
677 *Géotechnique Letters*, 4(3), 170-178.
678 Ozudogru, T.Y., Olgun, C.G., and Arson, C.F. (2015). "Analysis of friction induced thermo-
679 mechanical stresses on a heat exchanger pile in isothermal soil." *Geotechnical and*
680 Geological Engineering, 33(2), 357-371.
681 Pasten, C., and Santamarina, J. (2014). "Thermally induced long-term displacement of
682 thermoactive piles." J. Geotech. Geoenviron. Eng., 10.1061/(ASCE)GT.1943-
683 5606.0001092, 06014003.
684 Saggu, R. and Chakraborty, T. (2015). "Cyclic thermo-mechanical analysis of energy piles in
685 sand." *Geotechnical and Geological Engineering*, 33(2), 321-342.
686 Singh, R., Bouazza, A. and Wang, B. (2015). "Near-field ground thermal response to heating
687 of a geothermal energy pile: observations from a field test." *Soils and Foundations*,
688 55(6), 1412-1426.
689 Stewart, M. A. and McCartney, J. S. (2014). "Centrifuge modeling of soil-structure interaction
690 in energy foundations." *Journal of Geotechnical and Geoenvironmental Engineering*,
691 10.1061/(ASCE)GT.1943-5606.0001061, 04013044-1-11.
692 Suryatriyastuti, M. E., Mroueh, H., Burlon, S. (2013). "Numerical analysis of the bearing
693 capacity in thermo-active piles under cyclic axial loading." Energy geostructures:
694 Innovation in underground engineering, L. Laloui and A. Di Donna, eds., John Wiley,
695 Hoboken, NJ, 139–154.
696 Sutman, M., Olgun, C. G. and Brettmann, T. (2015). "Full-scale field testing of energy piles."
697 *IFCEE 2015*, ASCE, Texas, United States, 1638-1647.
698 Wang, B. (2017). "Behaviour of pile foundations subjected to thermal loading." Master of
699 Engineering Thesis, Monash University, Melbourne, Australia.

Wang, B., Bouazza, A., Singh, R., Haberfield, C., Barry-Macaulay, D. and Baycan, S. (2015). "Posttemperature effects on shaft capacity of a full-scale geothermal energy pile." *Journal of Geotechnical and Geoenvironmental Engineering*, 141 (4), 10.1061/(ASCE)GT.1943-5606.0001266, 04014125-1-12.

Wang, C., Liu, H., Kong, G., Ng, C. W. W. and Wu, D. (2016). "Model tests of energy piles with and without a vertical load." *Environmental Geotechnics*, 3(4), 203-213.

Wood, C. J., Liu, H. and Riffat, S. B. (2010). "Comparison of a modelled and field tested piled ground heat exchanger system for a residential building and the simulated effect of assisted ground heat recharge." *International Journal of Low-Carbon Technologies*, 5(3), 137-143.

Yavari, N., Tang, A. M., Pereira, J.M. and Hassen, G. (2014). "Experimental study on the mechanical behaviour of a heat exchanger pile using physical modelling." *Acta Geotechnica*, 9(3), 385-398.

Yavari, N., Tang, A. M., Pereira, J.M. and Hassen, G. (2016a). "Mechanical behaviour of a small-scale energy pile in saturated clay." *Géotechnique*, 66(11), 878-887.

Yavari, N., Tang, A. M., Pereira, J.M., and Hassen, G. (2016b). "Effect of temperature on the shear strength of soils and the soil–structure interface." *Canadian Geotechnical Journal*, 53(7), 1186-1194.

Yi, M., Hongxing, Y. and Zhaohong, F. (2008). "Study on hybrid ground-coupled heat pump systems." *Energy and Buildings*, 40(11), 2028-2036.

Yu, K. L., Singh, R. M., Bouazza, A. and Bui, H. H. (2015). "Determining soil thermal conductivity through numerical simulation of a heating test on a heat exchanger pile." *Geotechnical and Geological Engineering*, 33(2), 239-252.

Zhou, H., Kong, G., Liu, H., Wu, Y. and Li, G. (2016). "A novel cavity expansion-based analytical tool and its potential application for energy pile foundation." *Energy*

Geotechnics: Proceedings of the 1st International Conference on Energy Geotechnics, *ICEGT 2016, Kiel, Germany,* Wuttke A, Bauer S, and Sánchez, M, eds., CRC Press, London, UK, 359-365.

Table 1. Summary of ground conditions at the test site (Barry-Macaulay *et al.*, 2013; Singh *et al.*, 2015; Wang *et al.*, 2015; Yu *et al.*, 2015).

732

Depth (m)	Soil Type	Soil Description	In situ test values	Gravimetric water content (%)	Thermal conductivity (W/mK)*
0 – 1.5	Fill Material	Silty clay with traces of fine gravel and medium-coarse grained sand.	-	20 – 30	-
1.5 – 2.5	Sandy Clay	Clay containing fine-medium grained sand with cemented layers.	PP > 400 kPa	12 – 19	1.7
2.5 – 10.0	Sand (with traces of Clay)	Fine to coarse-grained sand. Dense from 2.5 m to 4 m and very dense from 4 m to 10 m. Quartz content ≤ 65%.	N = 26 @ 3 m depth N = HB > 3 m depth[a]	5 – 8	1.6 (at 8 m depth)
10 – 16.1	Sand	Fine to coarse-grained sand. Very dense. Quartz content = 93%.	N = HB[a]	2 – 5	2 – 2.2 (at 12 – 14 m depth)

733 * based on laboratory tests on soils recovered during the drilling process.

734 [a] HB (hammer bounce) encountered during SPT tests conducted i.e. N > 50.

735

736

737

738

739

740 **Table 2.** Summary of experiments.

Operating mode	Description	Inlet water temperatures	Inlet water flowrates	Experiment duration
24H	24 hours heating, daily.	45°C	10 LPM	52 Days
24C	24 hours cooling, daily.	5°C	15 LPM	24 Days
16N	16 hours cooling and 8 hours rest, daily.	5°C	15 LPM	25 Days
16F	16 hours cooling and 8 hours heating, daily.	7°C to 16°C in the cooling cycle. 30°C to 55°C in the heating cycle.	15 LPM in the cooling cycle. 13.5 LPM in the heating cycle	24 Days

741

742

743

744

745

746

747

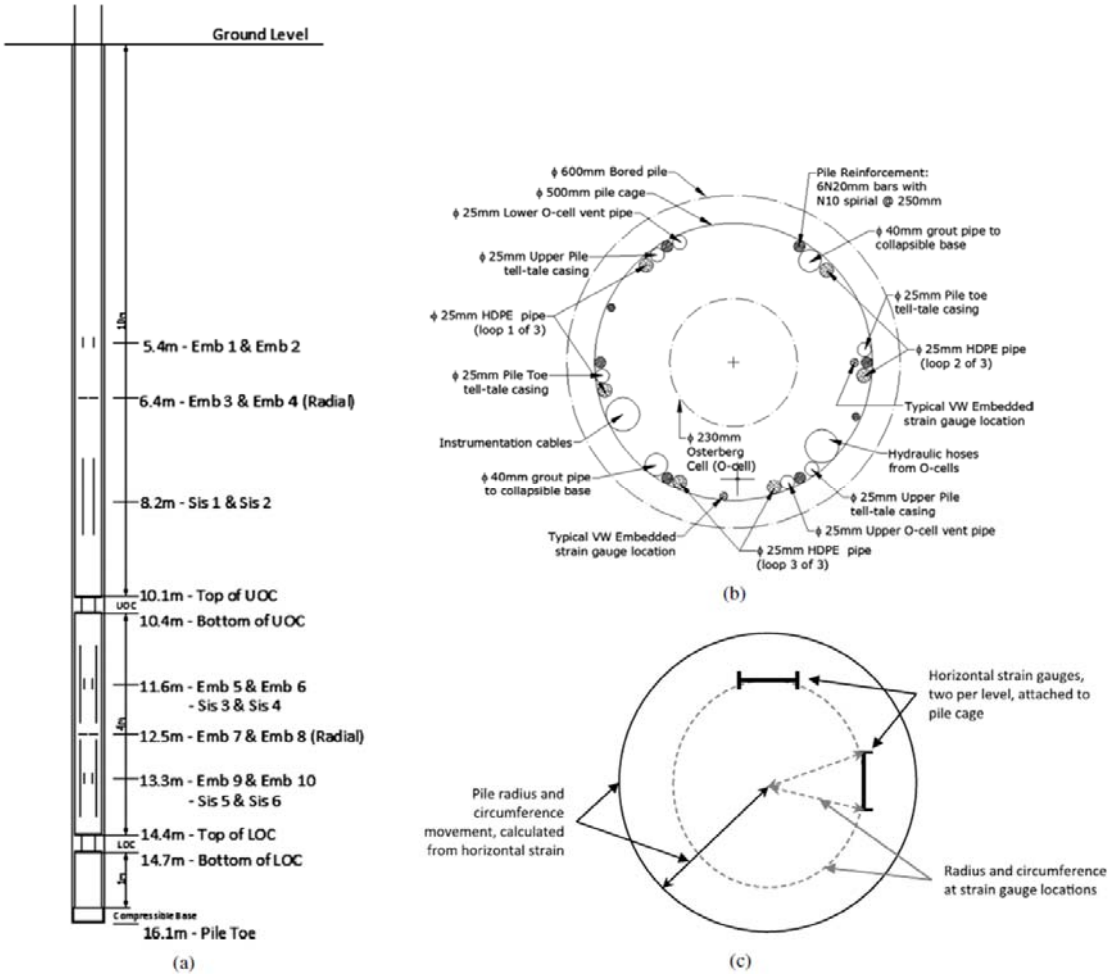

748

749

750 **Fig. 1. a)** Schematic diagram of the energy pile (LOC: lower O-cell, UOC: upper O-cell, Emb:
751 embedment strain gauge, Sis: sisters bar strain gauge), **b)** horizontal cross section of the energy
752 pile showing distribution of instrumentation, **c)** pile cross section at horizontal strain gauge
753 levels, 6.4 and 12.5 m below ground level (adapted from Wang *et al*., 2015).

754

755

756

757

758

759

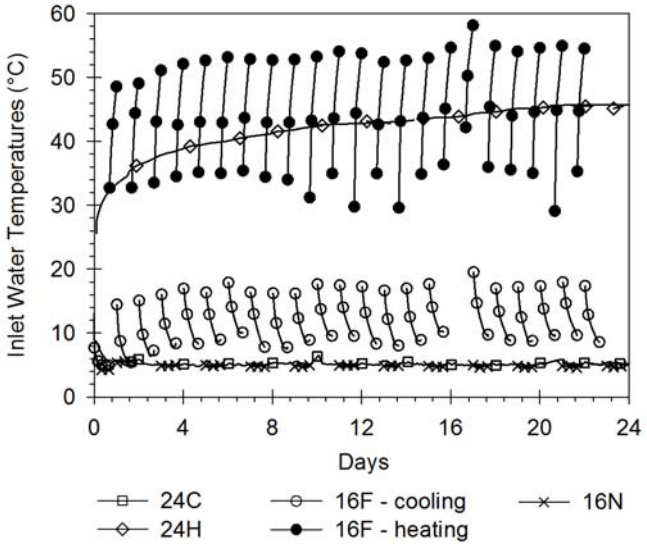

760

761

762 **Fig. 2.** Inlet water temperatures for the four experiments on the pile (24C: twenty-four hours
763 monotonic cooling; 24H: twenty-four hours monotonic heating; 16F: sixteen hours cooling
764 followed by eight hours heating; and 16N: sixteen hours cooling followed by eight hours rest).

765

766

767

768

769

770

771

772

773

774

775

776

777

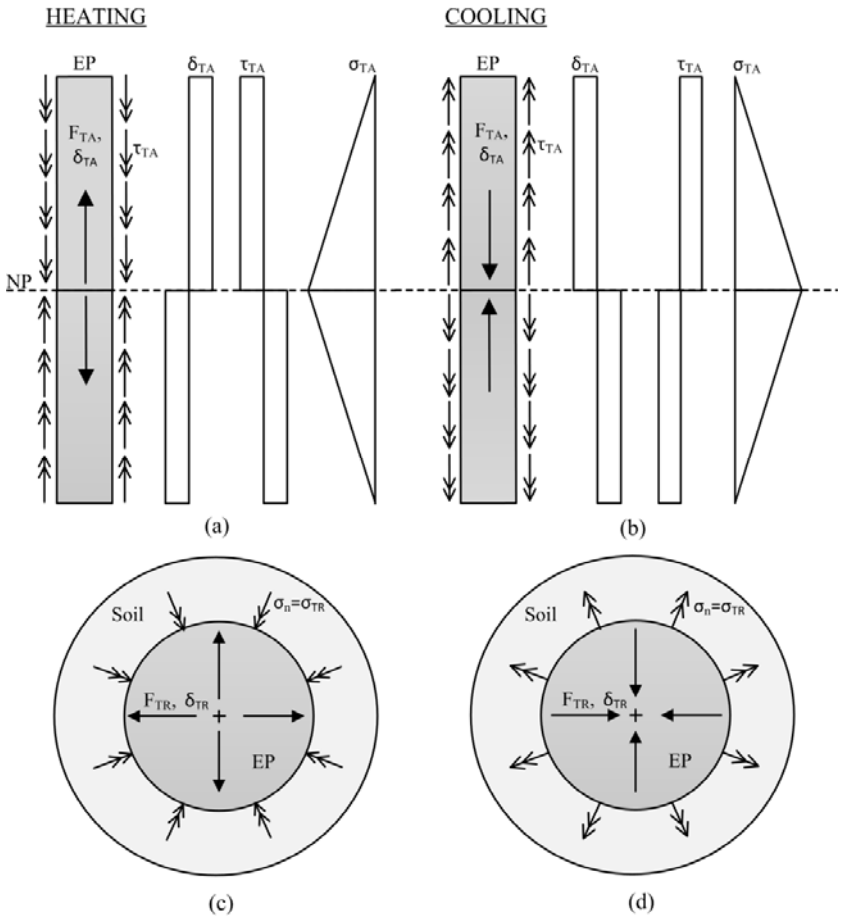

778

779 **Fig. 3.** Schematic of thermal response of an energy pile with free ends undergoing heating and
780 cooling (NP: null point, EP: energy pile, F_T: thermal force, δ_T: thermal displacement, τ_{TA}:
781 thermally induced side shear stress, σ_T: thermal stress, σ_n: normal stress, A: axial, R: radial):
782 **a)** axial response during heating, **b)** axial response during cooling, **c)** radial response during
783 heating, **d)** radial response during cooling.

784

785

786

787

788

789

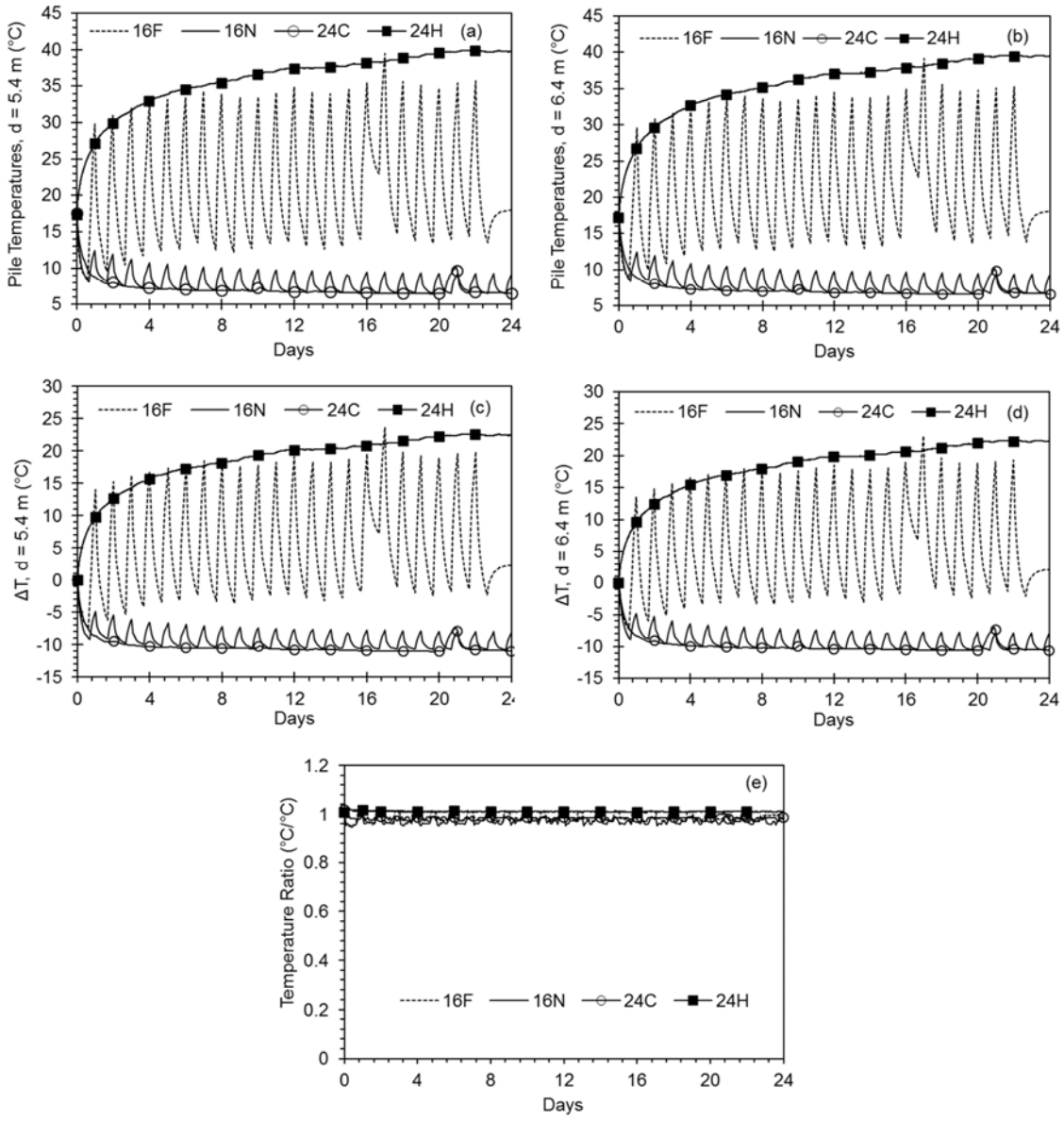

790

791 **Fig. 4.** Pile temperatures: **a)** at a depth of 5.4 m, **b)** at a depth of 6.4 m, **c)** change in pile

792 temperatures, ΔT, at a depth of 5.4 m, **d)** change in pile temperatures, ΔT, at a depth of 6.4 m,

793 **e)** ratio of pile temperatures measured at a depth of 5.4 m to a depth of 6.4 m.

794

795

796

797

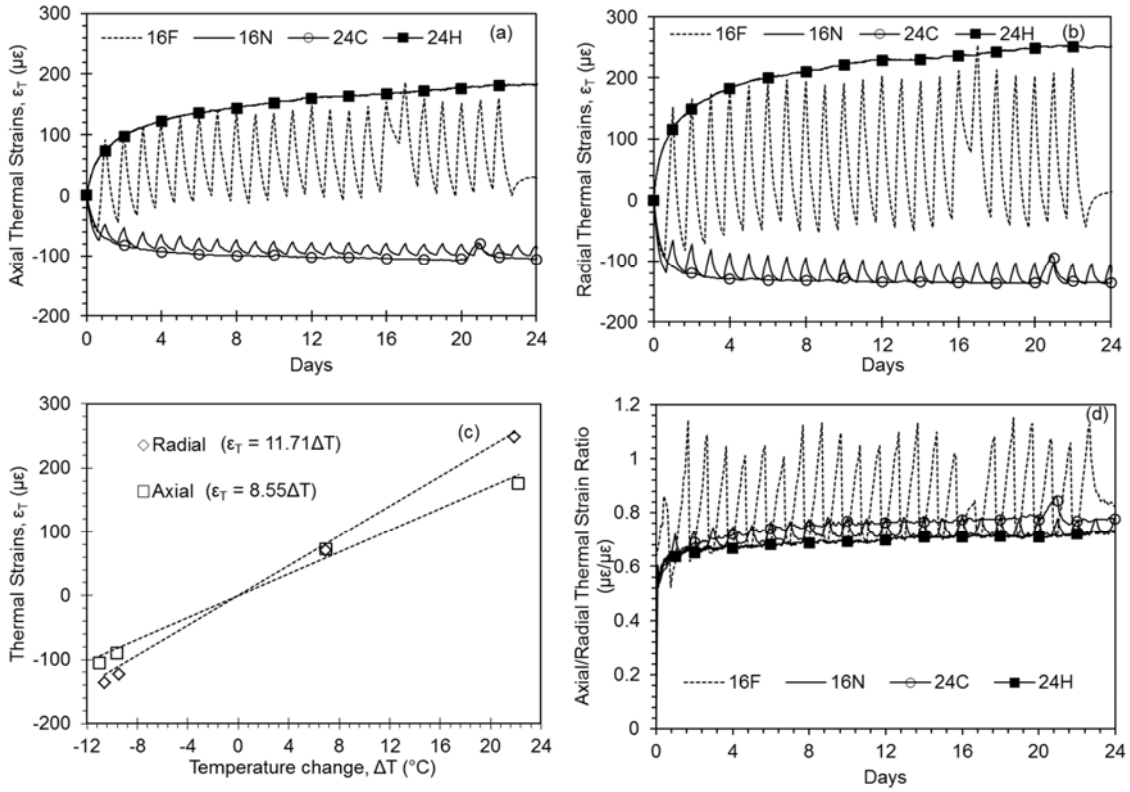

Fig. 5. Thermal strains: **a)** axial, **b)** radial, **c)** relationships between strains and temperature change, **d)** ratio of axial and radial thermal strains.

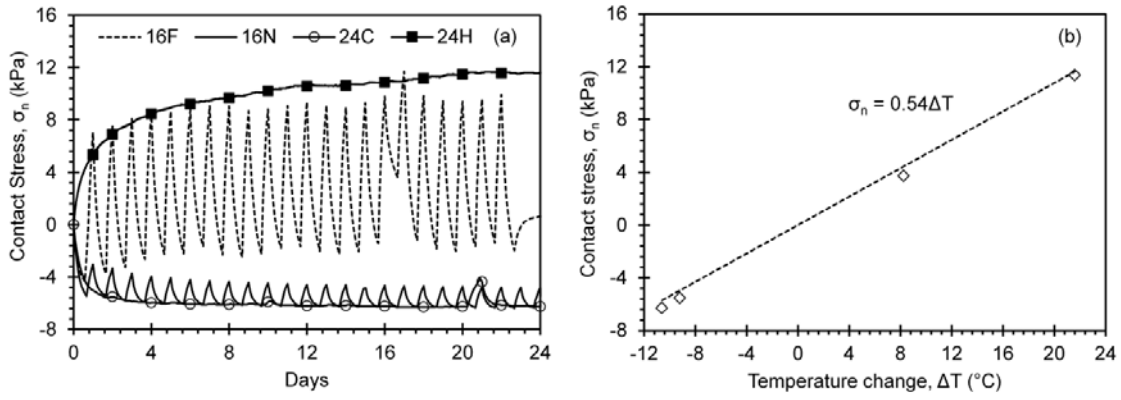

Fig. 6. Pile-soil radial contact stresses: **a)** transient, **b)** relationship between contact stress and temperature change.

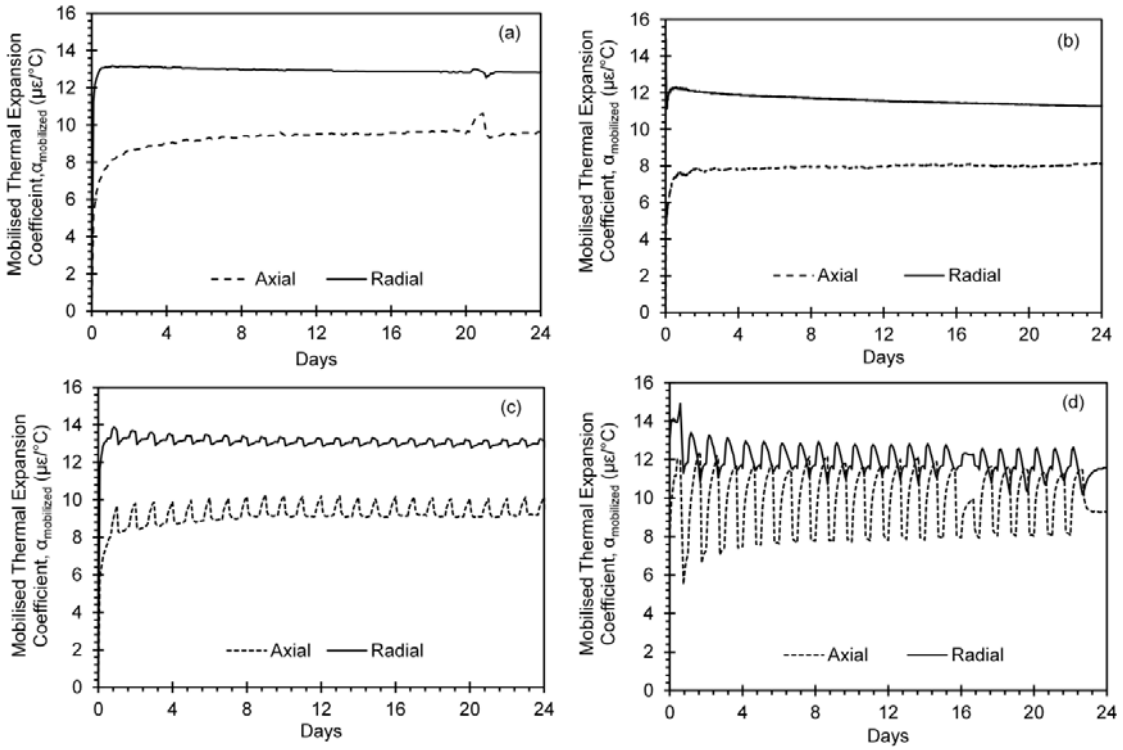

832

833 **Fig. 7.** Mobilized thermal expansion coefficients, $\alpha_{mobilized}$: **a**) 24C mode, **b**) 24H mode, **c**)

834 16N mode, **d**) 16F mode.

835

836

837

838

839

840

841

842

843

844

845

846

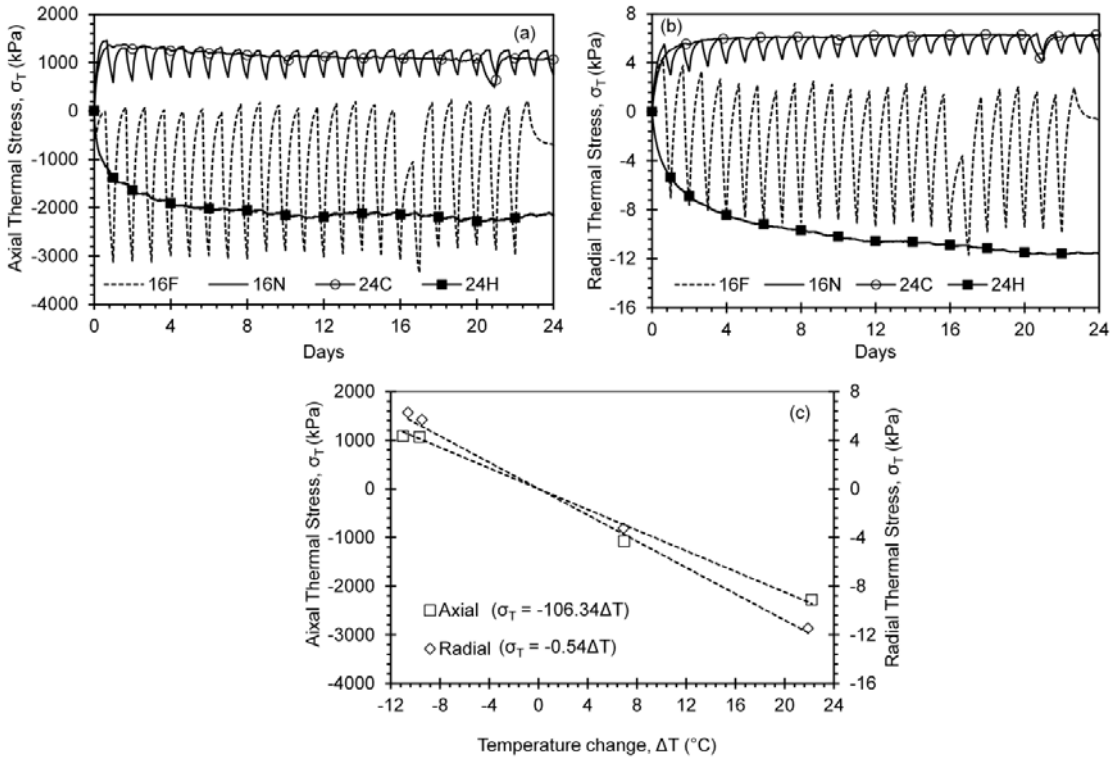

847

848 **Fig. 8.** Thermal stresses; **a**) axial, **b**) radial, **c**) relationships between thermal stresses and

849 temperature change.

850

851

852

853

854

855

856

857

858

859

860

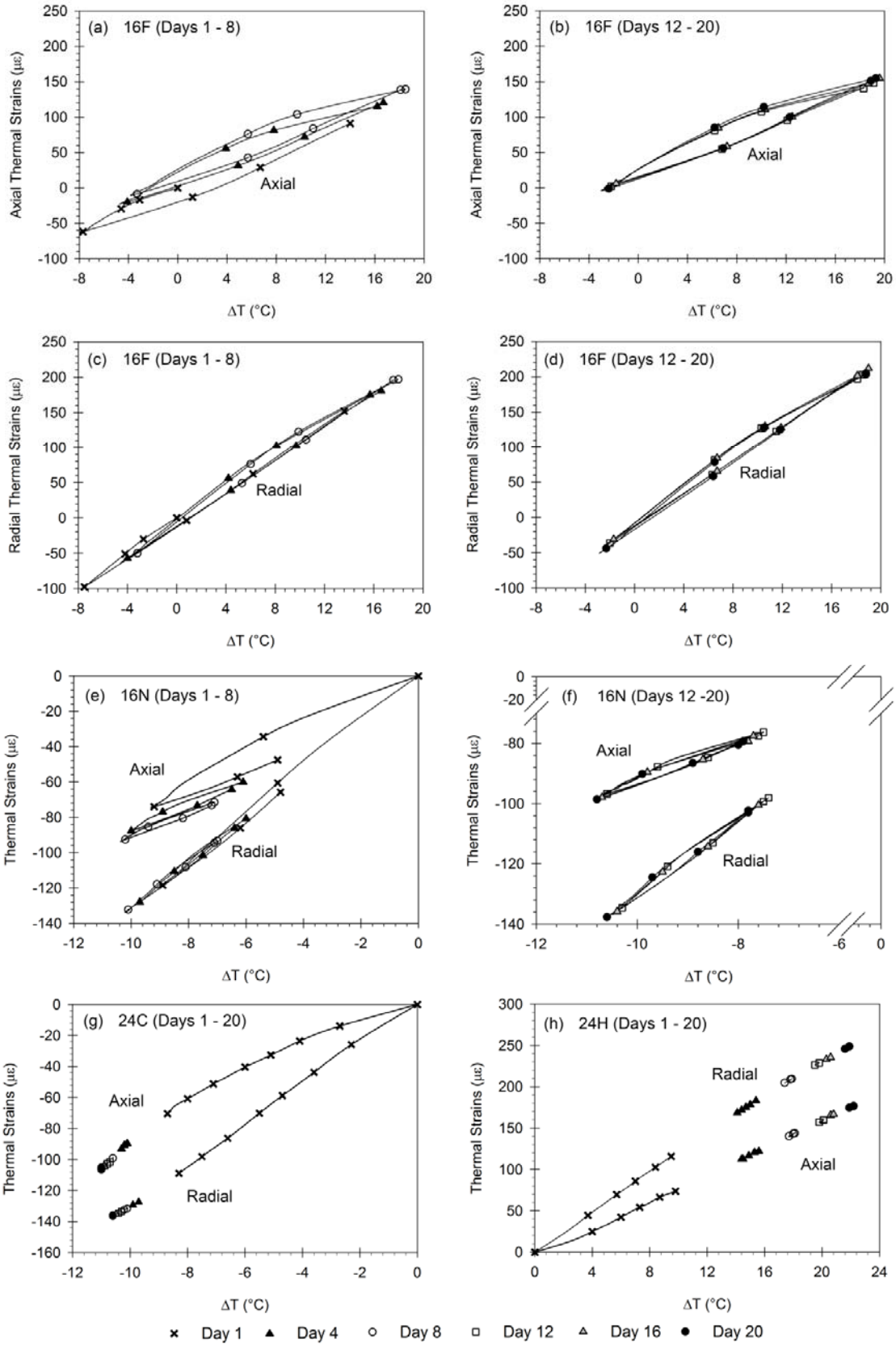
(a) 16F (Days 1 - 8)
Axial Thermal Strains (με)
Axial
ΔT (°C)
(b) 16F (Days 12 - 20)
Axial Thermal Strains (με)
Axial
ΔT (°C)
(c) 16F (Days 1 - 8)
Radial Thermal Strains (με)
Radial
ΔT (°C)
(d) 16F (Days 12 - 20)
Radial Thermal Strains (με)
Radial
ΔT (°C)
(e) 16N (Days 1 - 8)
Thermal Strains (με)
Axial
Radial
ΔT (°C)
(f) 16N (Days 12 -20)
Thermal Strains (με)
Axial
Radial
ΔT (°C)
(g) 24C (Days 1 - 20)
Thermal Strains (με)
Axial
Radial
ΔT (°C)
(h) 24H (Days 1 - 20)
Thermal Strains (με)
Radial
Axial
ΔT (°C)
Day 1
Day 4
Day 8
Day 12
Day 16
Day 20

861

Fig. 9. Axial and radial thermal strains plotted against ΔT; **a**) axial thermal strains between Days 1 – 8 for 16F mode, **b**) axial thermal strains between Days 12 – 20 for 16F mode, **c**) radial thermal strains between Days 1 – 8 for 16F mode, **d**) radial thermal strains between Days 12 – 20 for 16F mode, **e**) axial and radial thermal strains between Days 1 – 8 for 16N mode, **f**) axial and radial thermal strains between Days 12 – 20 for 16N mode, **g**) axial and radial thermal strains between Days 1 – 20 for 24C mode, **h**) axial and radial thermal strains between Days 1 – 20 for 24H mode.